EUROPEAN UROLOGY ONCOLOGY xxx (2021) xxx

available at www.sciencedirect.com
journal homepage: euoncology.europeanurology.com

European Association of Urology

Fibroblast Growth Factor Receptor 1 Drives the Metastatic Progression of Prostate Cancer

Estefania Labanca [a,b,c], *Jun Yang* [a,b], *Peter D.A. Shepherd* [a,b], *Xinhai Wan* [a,b], *Michael W. Starbuck* [a,b], *Leah D. Guerra* [a,b], *Nicolas Anselmino* [a,b], *Juan A. Bizzotto* [d,e], *Jiabin Dong* [a,b], *Arul M. Chinnaiyan* [f,g], *Murali K. Ravoori* [h], *Vikas Kundra* [h,i], *Bradley M. Broom* [j], *Paul G. Corn* [a,b], *Patricia Troncoso* [k], *Geraldine Gueron* [d,e], *Christopher J. Logothethis* [a,b], *Nora M. Navone* [a,b,*]

[a] *Department of Genitourinary Medical Oncology, The University of Texas MD Anderson Cancer Center, Houston, TX, USA;* [b] *David H. Koch Center for Applied Research of Genitourinary Cancers, The University of Texas MD Anderson Cancer Center, Houston, TX, USA;* [c] *The University of Texas MD Anderson Cancer Center UTHealth Graduate School of Biomedical Sciences, Houston, TX, USA;* [d] *Laboratorio de Inflamación y Cáncer, Departamento de Química Biológica, Facultad de Ciencias Exactas y Naturales, Universidad de Buenos Aires, Buenos Aires, Argentina;* [e] *Instituto de Química Biológica de la Facultad de Ciencias Exactas y Naturales (IQUIBICEN), CONICET-Universidad de Buenos Aires, Buenos Aires, Argentina;* [f] *Michigan Center for Translational Pathology, University of Michigan, Ann Arbor, MI, USA;* [g] *Department of Computational Medicine and Bioinformatics, University of Michigan, Ann Arbor, MI, USA;* [h] *Department of Cancer Systems Imaging, The University of Texas MD Anderson Cancer Center, Houston, TX, USA;* [i] *Diagnostic Radiology, The University of Texas MD Anderson Cancer Center, Houston, TX, USA;* [j] *Department of Bioinformatics and Computational Biology, The University of Texas MD Anderson Cancer Center, Houston, TX, USA;* [k] *Department of Pathology, The University of Texas MD Anderson Cancer Center, Houston, TX, USA*

Article info

Article history:
Received 7 July 2021
Received in Revised form
16 September 2021
Accepted October 4, 2021

Associate Editor:
Gianluca Giannarini

Keywords:
Bone metastasis
Fibroblast growth factor receptor 1
Ladinin 1
Prostate cancer

Abstract

Background: No curative therapy is currently available for metastatic prostate cancer (PCa). The diverse mechanisms of progression include fibroblast growth factor (FGF) axis activation.
Objective: To investigate the molecular and clinical implications of fibroblast growth factor receptor 1 (FGFR1) and its isoforms (α/β) in the pathogenesis of PCa bone metastases.
Design, setting, and participants: *In silico*, *in vitro*, and *in vivo* preclinical approaches were used. RNA-sequencing and immunohistochemical (IHC) studies in human samples were conducted.
Outcome measurements and statistical analysis: In mice, bone metastases (chi-square/Fisher's test) and survival (Mantel-Cox) were assessed. In human samples, FGFR1 and ladinin 1 (LAD1) analysis associated with PCa progression were evaluated (IHC studies, Fisher's test).
Results and limitations: FGFR1 isoform expression varied among PCa subtypes. Intracardiac injection of mice with FGFR1-expressing PC3 cells reduced mouse survival (α, $p < 0.0001$; β, $p = 0.032$) and increased the incidence of bone metastases (α, $p < 0.0001$; β, $p = 0.02$). Accordingly, IHC studies of human castration-resistant PCa (CRPC) bone metastases revealed significant enrichment of FGFR1 expression compared with treatment-naïve, nonmetastatic primary tumors ($p = 0.0007$). Expression of anchoring filament protein LAD1 increased in FGFR1-expressing PC3 cells and was enriched in human CRPC bone metastases ($p = 0.005$).
Conclusions: FGFR1 expression induces bone metastases experimentally and is significantly enriched in human CRPC bone metastases, supporting its prometastatic effect in PCa. LAD1 expression, found in the prometastatic PCa cells expressing FGFR1, was also

* Corresponding author. Department of Genitourinary Medical Oncology, MD Anderson Cancer Center, Unit 18-6, 1515 Holcombe, Boulevard, Houston, TX 77030, USA. Tel. +1 713 563 7273; Fax: +1 713 745 9880.
E-mail address: nnavone@mdanderson.org (N.M. Navone).

https://doi.org/10.1016/j.euo.2021.10.001

Please cite this article as: E. Labanca, J. Yang, Peter D.A. Shepherd et al., Fibroblast Growth Factor Receptor 1 Drives the Metastatic Progression of Prostate Cancer, Eur Urol Oncol (2021), https://doi.org/10.1016/j.euo.2021.10.001

enriched in CRPC bone metastases. Our studies support and provide a roadmap for the development of FGFR blockade for advanced PCa.

Patient summary: We studied the role of fibroblast growth factor receptor 1 (FGFR1) in prostate cancer (PCa) progression. We found that PCa cells with high FGFR1 expression increase metastases and that FGFR1 expression is increased in human PCa bone metastases, and identified genes that could participate in the metastases induced by FGFR1. These studies will help pinpoint PCa patients who use fibroblast growth factor to progress and will benefit by the inhibition of this pathway.

1. Introduction

Metastatic prostate cancer (PCa) that progresses after androgen ablation therapy (castration-resistant PCa [CRPC]) remains incurable [1]. The fibroblast growth factor (FGF) axis was implicated in PCa development and progression [2–5]. We previously reported that FGF receptor (FGFR) blockade with dovitinib (TKI258) has clinical activity in a subset of men with CRPC and bone metastases [6]. Subsequent reports support our findings implicating the FGF axis in PCa pathogenesis [7,8]. Currently, a phase 2 clinical trial using erdafitinib, a specific FGFR inhibitor, is underway for CRPC (Clinicaltrials.gov ID NCT03999515). Therefore, a deeper understanding of the FGF-mediated mechanisms underlying PCa progression is needed to refine FGFR blockade as a therapy for PCa.

The FGF axis consists of numerous receptor-binding ligands, receptor tyrosine kinases, and their isoforms. The FGFR1 extracellular ligand-binding region comprises two or three Ig-like domains, resulting from alternative splicing of the α-exon, leading to FGFR1α (containing the α-exon) and FGFR1β (lacking the α-exon) isoforms. These isoforms were associated with glioblastoma and pancreatic, breast, and bladder cancer [9–13], and were suggested to have different cellular effects: while FGFR1β was associated with tumorigenesis and poor survival [9–16], FGFR1α was implicated in cell differentiation [14,17]. Only FGFR1α was found in the nucleus, suggesting that IgI might be important for its nuclear targeting [18].

The focus of this study is to investigate the role of FGFR1 and its isoforms, α/β, in PCa bone growth and metastasis. Here, we report for the first time that the expression of FGFR1 isoforms varies among PCa cases and is associated with different gene signatures, and that FGFR1 accelerates PCa metastatic dissemination. We also found that ladinin 1 (LAD1), a relatively uncharacterized anchoring filament protein, is induced by FGFR1 expression and enriched in human PCa bone metastases. Results from our studies provide a framework for developing FGFR-targeted therapies for PCa and identification of markers of progression.

2. Patients and methods

2.1. Cell lines, patient-derived xenografts, and treatment

PC3 and C4-2B cells were purchased from the American Type Culture Collection (Manassas, VA, USA) and maintained in RPMI-1640 (Millipore Sigma, Burlington, MA, USA) supplemented with 10% FBS (Millipore Sigma).

FGFR1α and FGFR1β sublines were developed from parental cell lines by stably transfecting them with pcDNA3.1-FGFR1α-P2A-eGFP (PC3-FGFR1α and C4-2B–FGFR1α) or pcDNA3.1-FGFR1β-P2A-eGFP (PC3-FGFR1β and C4-2B–FGFR1β) plasmids (GenScript, Piscataway, NJ, USA). Control sublines (transfected with empty vectors, PC3-V and C4-2B–V) were also generated. Transfected cell lines were selected by treatment with G418 (Geneticin, Sigma-Aldrich, St. Louis, MO, USA) *in vitro* and subsequent cell sorting for GFP expression by fluorescence-activated cell sorting (FACS).

Luciferase-expressing sublines of C4-2B–FGFR1α, C4-2B–FGFR1β, and V were generated by infection with CMV-luciferase(firefly)-2A-RFP virus vector (AMSBIO, Abingdon, UK) followed by selection with puromycin (Thermo Scientific, Waltham, MA, USA) and FACS as described above.

LAD1 silencing in PC3-V and PC3-FGFR1β was performed by using pRFP-CB-shLenti shRNA lentiviral particles (shLAD1) or Scramble shRNA (Scr) as control (Origene, Rockville, MD, USA), followed by blasticidin (Invivogen, San Diego, CA, USA) selection.

2.1.1. Patient-derived xenograft

MDA PCa 118b was previously developed in our laboratory [19].

2.1.2. Cell treatment

PC3, C4-2B stably expressing FGFR1 isoforms, and empty vector controls were serum starved for 3 h, and 50 ng/ml heparan sulfate proteoglycan (Sigma-Aldrich) was added during the last hour. Then we added 100 μg/ml FGF2 or FGF9 (Peprotech, Cranbury, NJ, USA) for 45 min to activate the FGFR pathway. Untreated cells were used as controls.

2.2. Western blot analysis

Cells treated as outlined above were harvested at the end of treatment, and total cell lysates were used for immunoblot analysis as described previously [6]. Antibodies used are described in the Supplementary material.

2.3. Reverse-phase protein array

Reverse-phase protein array (RPPA) was performed as described previously [20].

2.4. Animals

2.4.1. Intrabone assays

Cells were injected into the distal end of femurs of 6- to 8-wk-old male CB17.SCID mice, as described previously [3]. All femurs of injected mice were monitored by x-ray imaging. Quantification of the radiolucent

Please cite this article as: E. Labanca, J. Yang, Peter D.A. Shepherd et al., Fibroblast Growth Factor Receptor 1 Drives the Metastatic Progression of Prostate Cancer, Eur Urol Oncol (2021), https://doi.org/10.1016/j.euo.2021.10.001

areas of the x-ray analyses were obtained as the ratio of radiolucent area to the total tissue area (whole bone) using BioQuant Osteo (BIOQUANT, Nashville, TN, USA).

2.4.2. Intracardiac injection

Cells were injected into the left ventricle of 6- to 8-wk-old male CB17. SCID mice. Bone reaction and bone metastasis development were monitored by x-ray and micro–computed tomography (μCT).

Additional details are described in the Supplementary material.

All practices involving laboratory animals were approved by the Institutional Animal Care and Use Committee of MD Anderson, Houston, TX, under the regulation of the Animal Welfare Committee (IACUC), and conform to the NIH Policy on Humane Care and Use of Laboratory Animals.

2.5. Bone histomorphometric analysis

Histomorphometric analyses were performed at the Bone Histomorphometry Core Laboratory, The Bone Disease Program of Texas, Houston, TX, USA, as described previously [3]. Bone parameters (bone mass, osteoblast, and osteoclast) were obtained using tartrate-resistant acid phosphatase stains and Harris-modified hematoxylin counterstain of decalcified bones.

2.6. Immunohistochemical analyses in human prostate and PCa specimens

We performed immunohistochemical (IHC) analyses of FGFR1 and LAD1 expression in PCa samples and of FGFR1 expression in normal prostate-derived tissue, obtained from the Prostate Tissue Bank, Department of Pathology, MD Anderson Cancer Center, Houston, TX, USA, under an Institutional Review Board–approved protocol. PCa tissue specimens were derived from the peripheral zone of nonmetastatic, untreated, primary PCa (seven, Gleason score 8; 23, Gleason score 9 [ten, pT2 and 20, pT3]), and from CRPC bone metastases.

Bone metastasis specimens were decalcified, and formalin fixed and paraffin embedded; all samples were stained with an anti-FGFR1 antibody (Cat# ab76464; Abcam, Cambridge, UK) and an anti-LAD1 antibody (Cat# HPA028732; Sigma-Aldrich), as described elsewhere [6]. Slides were read independently by two investigators and classified according to staining intensity, with – being negative stain and +++ being the most intense staining. Positive/negative (+/–) expression refers to heterogeneous expression, that is, some areas positive and some areas negative within the same sample, or very slight staining.

2.7. Bioinformatics analysis

Human RNA-sequencing data from the following datasets were used: TCGA-PRAD, containing gene expression data from primary PCa samples [21], and SU2C-PCF that has mRNA expression (FPKM capture) for CRPC samples [22].

TCGA-PRAD was mined for expression of FGFR1 isoforms and their molecular correlates (476 samples, last access: December 2018) [23]. Search was performed using FGFR1 isoforms (α NM_023110.2; and β, NM_023105.2). FGFR1 score was defined as the ratio of FGFR1α to the sum of FGFR1α and FGFR1β [24]. Gene set enrichment analysis (GSEA) was used to determine FGFR1-associated pathways [25].

SU2C-PCF detailed analysis is provided in the Supplementary material.

2.8. Statistical analysis

Two experimental groups were compared with the two-tailed Student's *t* test for unpaired data, unless otherwise indicated. Differences in FGFR1 isoform expression between metastatic tissue sites in SU2C were assessed by one-way analysis of variance followed by Dunnett's multiple comparisons test. Mantel-Cox test (logrank-Cox proportional hazard model) was employed for the analyses of Kaplan-Meier survival curves using survminer R package (R Foundation for Statistical Computing, Vienna, Austria) [26] or GraphPad Prism 8.4 (GraphPad Software Inc., San Diego, CA, USA). Chi-square or Fisher's exact tests were used to compare the number of mice with bone metastases. Fisher's exact test was used to compare IHC scores in human samples. All p values < 0.05 were considered statistically significant. Detailed information is available in the Supplementary material.

3. Results

3.1. Different human PCa samples express different FGFR1 isoforms

FGFR1 has the highest expression among all FGFRs in human PCa samples [6]. Herein, we show that different FGFR1 isoforms are expressed in different PCa samples (Supplementary Table 1). We focused this study on the two best characterized FGFR1 isoforms, α (containing the α-exon; NM_023110.2; 822 aa) and β (lacking the α-exon; NM_023105.2; 733 aa) [27,28]. When mining TCGA-PRAD and SU2C [22], results confirmed that both isoforms are expressed at different levels in different PCa samples (Supplementary Fig. 1A and 1B).

3.2. FGFR1 isoforms are associated with different gene expression

The TCGA-PRAD analysis revealed that FGFR1α and FGFR1β are associated with the expression of different gene transcripts, with FGFR1β being associated with a larger number of genes than FGFR1α (Fig. 1A and 1B). Accordingly, GSEA indicated that FGFR1β is associated with a larger number of pathways than FGFR1α (Fig. 1C, and Supplementary Tables 2 and 3). When the stringency of prioritized pathways was increased, we identified only one pathway associated with FGFR1α (Fig. 1D), while 50 pathways were associated with FGFR1β (Fig. 1E).

Supporting our *in silico* finding that the MAPK cascade is significantly associated with the β isoform (Fig. 1E), we used PC3 (hormone insensitive) and C4-2B (hormone sensitive) cell lines stably expressing FGFR1 isoforms (PC3-FGFR1α, PC3-FGFR1β; C4-2B–FGFR1α, C4-2B–FGFR1β) or empty vector (V) and treated with FGF (Fig. 1F, and Supplementary Fig. 2A and 2B), and observed greater induction of P-MAPK in FGFR1β-expressing cells (Fig. 1G). This was confirmed by RPPA of C4-2B cells stably expressing FGFR1 isoforms (Fig. 1H).

3.3. FGFR1 alters the bone phenotype induced by PCa cells in tumor-bearing femurs

Next, we evaluated tumor growth and bone reaction induced by PC3-FGFR1α or PC3-FGFR1β after direct femur injection (Fig. 2A). After 4 wk, radiolucent areas (α, p = 0.009; β, p = 0.0001; Fig. 2B) and tumor volume (α, p = 0.0006, β; p = 0.002; Fig. 2C) were increased and bone volume was reduced (α, p = 0.01; β, p = 0.007; Fig. 2D) in femurs injected with PC3-FGFR1 isoform tumors compared with PC3-V–injected femurs, indicating that FGFR1 expres-

Please cite this article as: E. Labanca, J. Yang, Peter D.A. Shepherd et al., Fibroblast Growth Factor Receptor 1 Drives the Metastatic Progression of Prostate Cancer, Eur Urol Oncol (2021), https://doi.org/10.1016/j.euo.2021.10.001

A Heatmap of top 2000 genes differentially correlated with FGFR1 isoforms

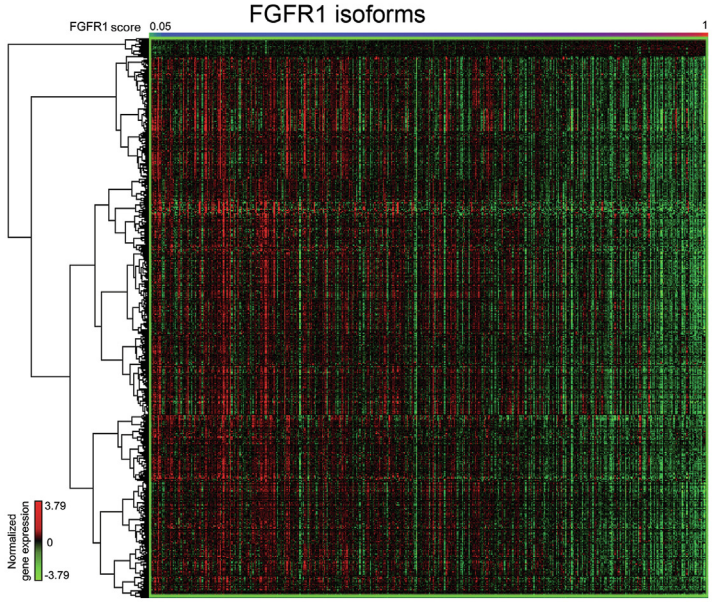

B Top 20 genes with the highest correlation to FGFR1 isoforms

Genes correlated to FGFR1α			Genes correlated to FGFR1β		
Gene	Correlation	Coefficient	Gene	Correlation	Coefficient
PLEKHH1	0.376033	2.526000	*PMP22*	0.564165	3.928847
THTPA	0.374498	1.036541	*CORO1C*	0.561130	2.550176
SLC25A42	0.365162	1.693602	*SERPING1*	0.559327	4.199745
PSD4	0.363058	1.231595	*FBLN5*	0.555418	4.084689
CANT1	0.360520	1.342872	*C1S*	0.554168	4.465541
LANCL2	0.347292	0.821909	*GLT8D2*	0.552024	3.920179
SPTBN2	0.338606	1.528507	*SYNPO*	0.548669	3.730633
SLC35E1	0.330903	1.004822	*IGFBP7*	0.547949	3.541869
CNNM3	0.328732	0.841545	*RAB31*	0.546616	3.504471
ATP13A2	0.327998	1.095434	*TNFAIP8L3*	0.545257	4.440794
KIAA0319L	0.327459	1.154684	*RFTN1*	0.543428	3.650135
C15orf37	0.326560	1.513964	*A2M*	0.542829	4.033372
ALG6	0.326037	1.221266	*CTSK*	0.539713	3.846549
CREB3L4	0.324394	1.362966	*C3orf59*	0.533698	3.347806
TTLL12	0.324218	1.211428	*TIMP2*	0.532424	3.359562
INTS5	0.324189	0.722684	*C1R*	0.531048	4.142481
MOGS	0.323972	0.884953	*LHFP*	0.527056	3.146070
LOC401588	0.318918	1.268518	*CLIC2*	0.526791	3.077692
UAP1	0.317344	1.636116	*CALHM2*	0.526377	2.984523
KIAA1543	0.316995	1.183821	*MFAP4*	0.526101	4.593608

C Proportion of pathways associated with FGFR1 isoforms

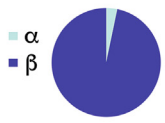

D Pathway most significantly associated to FGFR1α

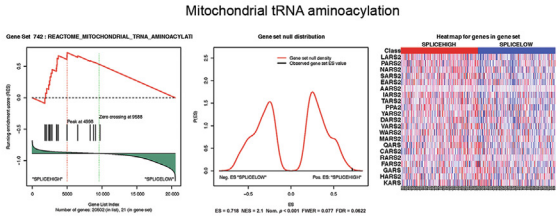

E Examples of pathways most significantly associated with FGFR1β

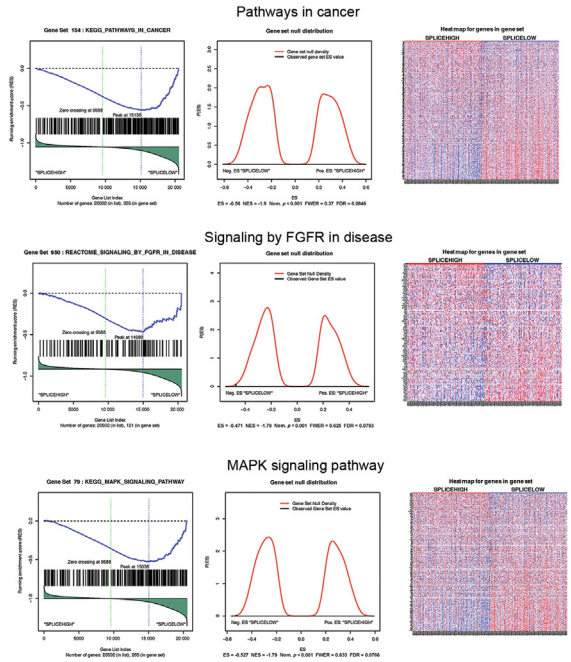

F Outline of cell preparation

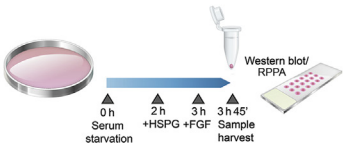

G Western blot analysis

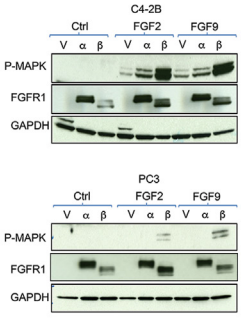

H RPPA's heatmap

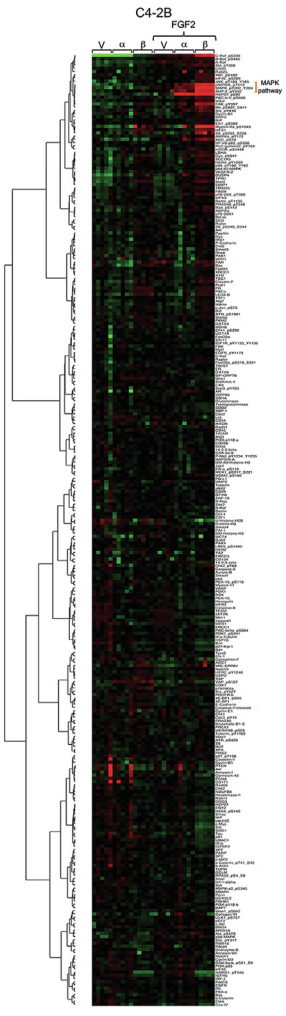

sion in PCa cells induces tumor growth and bone resorption. Bone mass reduction in PC3-FGFR1 isoform tumor-bearing femurs was confirmed by histomorphometry (α, $p = 0.0006$; β, $p = 0.004$; Fig. 2E); with a significant increase in osteoclast parameters only in PC3-FGFR1β–injected femurs (Fig. 2E).

We next evaluated the effect of FGFR1 isoform expression in C4-2B cells (Fig. 3A and 3B). No difference in tumor

volume was observed between C4-2B–FGFR1 isoforms and C4-2B–V groups (Fig. 3C). Bone volume decreased only in femurs injected with C4-2B–FGFR1β compared with controls (p = 0.02; Fig. 3D), with a concomitant increase in osteoclast parameters (p = 0.036; Fig. 3E).

These results suggest that FGFR1β-expressing PCa cells are more suited to activate osteoclasts.

3.4. FGFR1 significantly increases PCa bone metastases in vivo

In a survival study, mice injected intracardially with either PC3-FGFR1α or PC3-FGFR1β had reduced survival compared with controls (p < 0.0001 or p = 0.032, respectively; Fig. 4A).

Bone metastases after intracardiac injection of these sublines were monitored by x-ray and confirmed by histology when the study concluded (Fig. 4B–D). An increased number of mice injected with PC3-FGFR1α and PC3-FGFR1β developed bone metastases, compared with controls (p = 0.00005 and p = 0.02, respectively; Fig. 4C [bottom]). These results suggest that in androgen receptor (AR)-negative cells (PC3), FGFR1 mediates PCa progression.

FGFR1 isoform expression in C4-2B cells (AR expressing) did not increase bone metastases (Fig. 4E–F), indicating different FGFR1 prometastatic effects in different cell lines.

Taken together, these results suggest that both the isoforms and the genetic background of cells modulate the FGFR1 effect in PCa.

3.5. FGFR1 expression is significantly increased in human PCa metastases and negatively correlated with AR

FGFR1 enrichment in human CRPC bone metastases (11/26) versus untreated, nonmetastatic primary PCa (two out of 29) was detected by IHC analyses (p = 0.0007; Fig. 5, Supplementary Table 4, and Supplementary Fig. 2C), supporting that FGFR1 induces the PCa metastatic cascade. We found an increase in FGFR1 transcripts after androgen deprivation therapy (ADT) when assessing locally advanced/metastatic PCa patient–paired samples (GSE51005-GSE48403, p < 0.001; Supplementary Fig. 3A). Of note, FGFR1 mRNA and AR score were inversely associated (r = –0.42, p < 0.0001; Supplementary Fig. 3B) in SU2C [22]. Accordingly, we ascertained a negative correlation between FGFR1 and AR (r = –0.38, p < 0.0001; Supplementary Fig. 3C) in 39 CRPC MDA PCa patient-derived xenografts (PDXs) [19,29].

Strikingly, in SU2C, FGFR1β transcript expression was increased in bone metastasis compared with liver and lymph node (p = 0.006 and p = 0.0007, respectively; Supplementary Fig. 1B). These results suggest that cells expressing FGFR1β have more affinity for bone or that, once these cells are in the bone, they upregulate the expression of this isoform.

3.6. FGFR1 induces LAD1, an anchoring filament protein, in PC3 cells

To understand the mechanism of FGFR1-induced metastases, we performed RPPA of PC3-FGFR1 cells (Fig. 6A) and found that FGFR1 modulates genes associated with cellular movement (Fig. 6B), prioritizing those genes implicated in cancer progression and/or PCa (*LAD1*, *CDH1*, and *GLS*) [30–34]. We confirmed LAD1 upregulation in PC3-FGFR1 cells (Fig. 6C). LAD1 was enriched in human CRPC bone metastases compared with treatment-naïve, nonmetastatic primary tumors (p = 0.005; Fig. 6D and Supplementary Table 4), supporting that LAD1 mediates, at least in part, PCa metastasis.

3.7. LAD1 silencing in FGFR1β-overexpressing tumors reduces bone metastases

We assessed bone metastases in mice intracardially injected with PC3 cells overexpressing FGFR1β and with silenced

Fig. 1 – FGFR1 isoforms are associated with the expression of different genes in human prostate cancer. (A) Heatmap of the 2000 genes most highly correlated with FGFR1 isoforms α and β in the TCGA-PRAD dataset. The relative expression of each isoform was defined as the proportion of FGFR1α to the sum of FGFR1α + FGFR1β (FGFR1 score) in tumor samples (upper bar; a high ratio indicates the prevalence of the α isoform and a low ratio indicates the prevalence of the β isoform). Rows represent specific genes and columns represent tumor samples arranged in relative levels of FGFR1 isoforms. As the proportion of FGFR1α increased within the samples, expression of most genes decreased. The red color indicates high normalized gene expression and green low normalized gene expression. (B) List of the 20 genes most highly correlated with α and β isoforms of FGFR1 in the TCGA-PRAD dataset. The relative expression of each isoform was defined as the proportion of FGFR1α to the sum of FGFR1α + FGFR1β (FGFR1 score). The column head: Gene represents gene symbol, Correlation represents correlation coefficient, and Coefficient represents the magnitude of change in gene expression from FGFR1 score 0 (prevalence of FGFR1β) to 1 (prevalence of FGFR1α). (C) Pie chart representing the proportion of pathways significantly associated with FGFR1α (light blue) and FGFR1β (dark blue) resulting from the GSEA of FGFR1 isoforms in the TCGA-PRAD dataset. FGFR1β is associated with a larger number of pathways than FGFR1α (FGFR1α, n = 22; FGFR1β, n = 749). (D) The most significant FGFR1α (SPLICEHIGH)-associated pathway identified in the GSEA of the TCGA-PRAD dataset. FGFR1 score was defined as the ratio of FGFR1α to the sum of FGFR1α and FGFR1β. Samples were divided evenly into SPLICELOW and SPLICEHIGH subgroups based on the FGFR1 score. The selection criteria were the combined p < 0.002 and normalized enrichment score (NES) > 1.78. Only one pathway significantly associated with FGFR1α met these criteria (mitochondrial tRNA aminoacylation). (E) Pathways most significantly associated with FGFR1β (SPLICELOW) in the GSEA of the TCGA-PRAD dataset. FGFR1 score was defined as the ratio of FGFR1α to the sum of FGFR1α and FGFR1β. Samples were divided evenly into SPLICELOW and SPLICEHIGH subgroups based on the FGFR1 score. The selection criteria were the combined p < 0.002 and NES < –1.78. Fifty pathways were found to be significantly associated with FGFR1β under these criteria; the figure shows particular pathways of interest selected (MAPK signaling cascade, signaling by FGFR in disease, and pathways in cancer). (F) Schematic representation of the experimental protocol for cell preparation. PC3- or C4-2B–FGFR1α, FGFR1β, and control (V) cells were cultured in serum-starved conditions for 3 h, and heparan sulfate (HSPG, 50 ng/ml) was added during the last hour. Subsequently, cells were cultured in the absence or presence of 100 μg/ml FGF2 and/or FGF9 for 45 min. Then, cells were harvested and lysates were prepared for Western blot or RPPA. (G) Western blot analyses of FGFR1 and P-MAPK (Thr202/Tyr204) expression in C4-2B and PC3 cells expressing FGFR1α, FGFR1β, or empty vector (V), untreated or treated with FGF2 and FGF9 as outlined in (F). Similar results were obtained in independent experiments. GAPDH was used as a loading control. (H) Heatmap depicting antibody unsupervised hierarchical clustering of RPPA study results of C4-2B–FGFR1α, C4-2B–FGFR1β, and control (V) cells treated or untreated with FGF2. Cell lysates were prepared as outlined in (F). Each column represents a replicate (n = 5 per group). "Red" color in the heatmap indicates that the values are above the median, and "green" indicates that the values are below the median. Ctrl = control; ES = enrichment score; FDR = false discovery rate; FGF = fibroblast growth factor; FGFR = fibroblast growth factor receptor; FWER = family-wise error rate; GSEA = gene set enrichment analysis; Neg. = negative; Nom. = nominal; Pos. = positive; RPPA = reverse-phase protein array.

Please cite this article as: E. Labanca, J. Yang, Peter D.A. Shepherd et al., Fibroblast Growth Factor Receptor 1 Drives the Metastatic Progression of Prostate Cancer, Eur Urol Oncol (2021), https://doi.org/10.1016/j.euo.2021.10.001

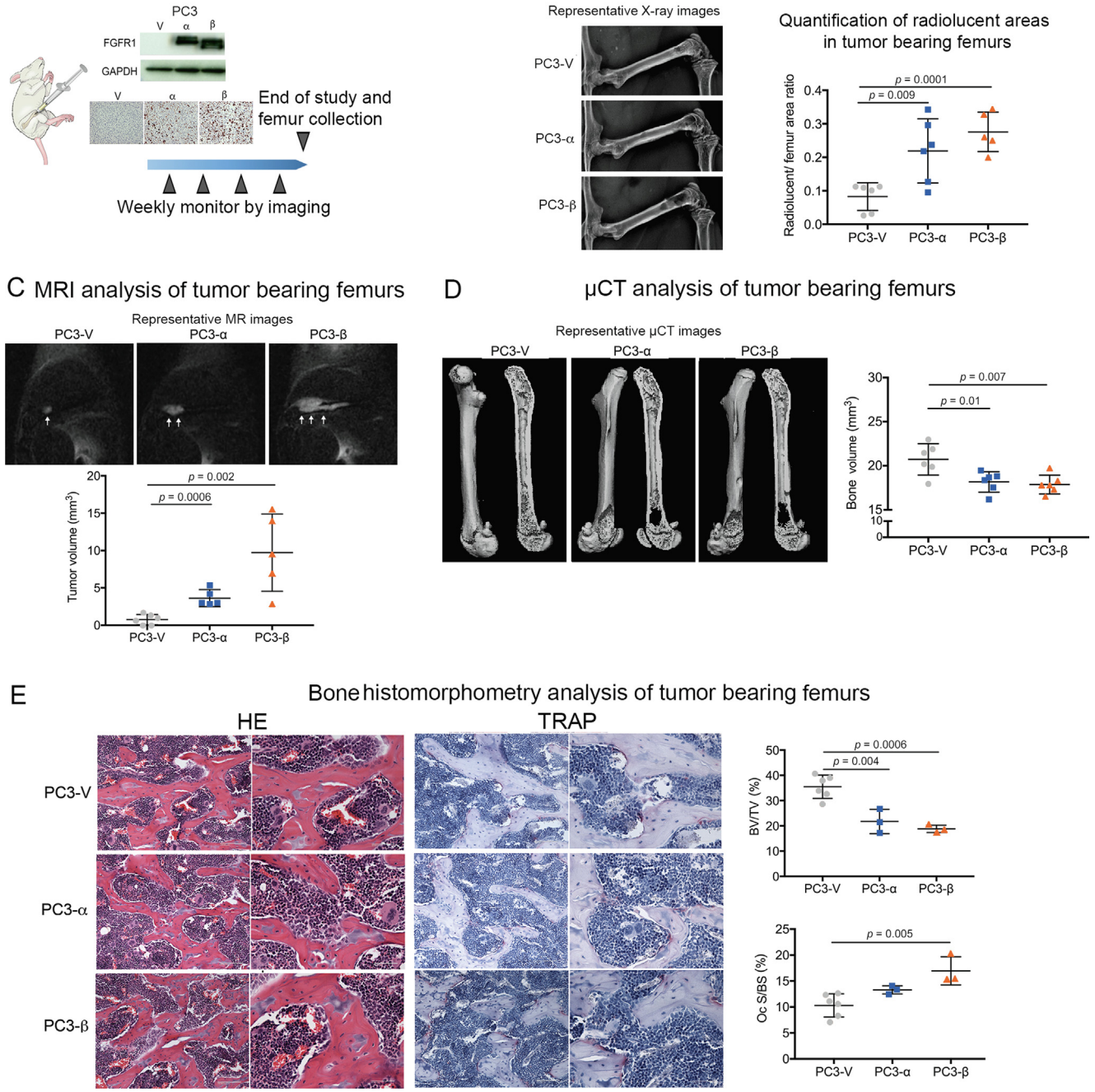

Fig. 2 – FGFR1 alters the bone phenotype induced by PC3 cells in tumor-bearing femurs. (A) Schematic representation of femur injection of PC3-FGFR1α, PC3-FGFR1β, or control empty vector (V) cells and monitoring. Western blot analysis and immunocytochemistry results of FGFR1 expression in cells used in these studies. GAPDH was used as a loading control in the Western blot analysis. Injected mice (*n* = 6 per group) were monitored by x-ray and MRI. (B) Representative radiographs (left panel) and quantification of radiolucent areas (right panel) of the x-ray analysis of PC3-FGFR1α, PC3-FGFR1β, and V tumor-bearing femurs at 4 wk after injection. Student's *t* test; error bars indicate SD. (C) Representative sagittal MR images of femurs acquired with a 4.7-T scanner using a T2-weighted fast spin (T2-FS) echo sequence with fat suppression (upper panel). Arrows indicate tumor, which appears as an area of increased signal on T2-weighted images. Tumor volume of PC3-FGFR1α, PC3-FGFR1β, or V tumor-bearing femurs was assessed by MRI analysis (lower panel). Student's *t* test; error bars indicate SD. (D) Representative two-dimensional slices of specimens analyzed by high-resolution µCT analysis at the end of study (left panel). Bone volume results assessed by µCT analysis (right panel). Student's *t* test; error bars indicate SD. (E) Representative photomicrographs of decalcified tumor-bearing femur sections stained with HE (left panel) and tartrate-resistant acid phosphatase (TRAP; middle panel; 20× magnification, left; 40× magnification, right). Bone histomorphometry analyses indicated a reduced ratio of bone volume to tissue volume (BV/TV) in PC3-FGFR1 tumor-bearing mice (upper right panel). Bone histomorphometry analyses of TRAP-stained sections indicate an increase in osteoclast (OC) surface/bone surface in PC3-FGFR1β tumor-bearing mice (lower right panel). Scale bar, 100 µm (20×) or 50 µm (40×). Student's *t* test; error bars indicate SD. FGFR = fibroblast growth factor receptor; HE = hematoxylin and eosin; µCT = micro–computed tomography; MRI = magnetic resonance imaging; OC S/BS = osteoclast surface/bone surface; SD = standard deviation.

Please cite this article as: E. Labanca, J. Yang, Peter D.A. Shepherd et al., Fibroblast Growth Factor Receptor 1 Drives the Metastatic Progression of Prostate Cancer, Eur Urol Oncol (2021), https://doi.org/10.1016/j.euo.2021.10.001

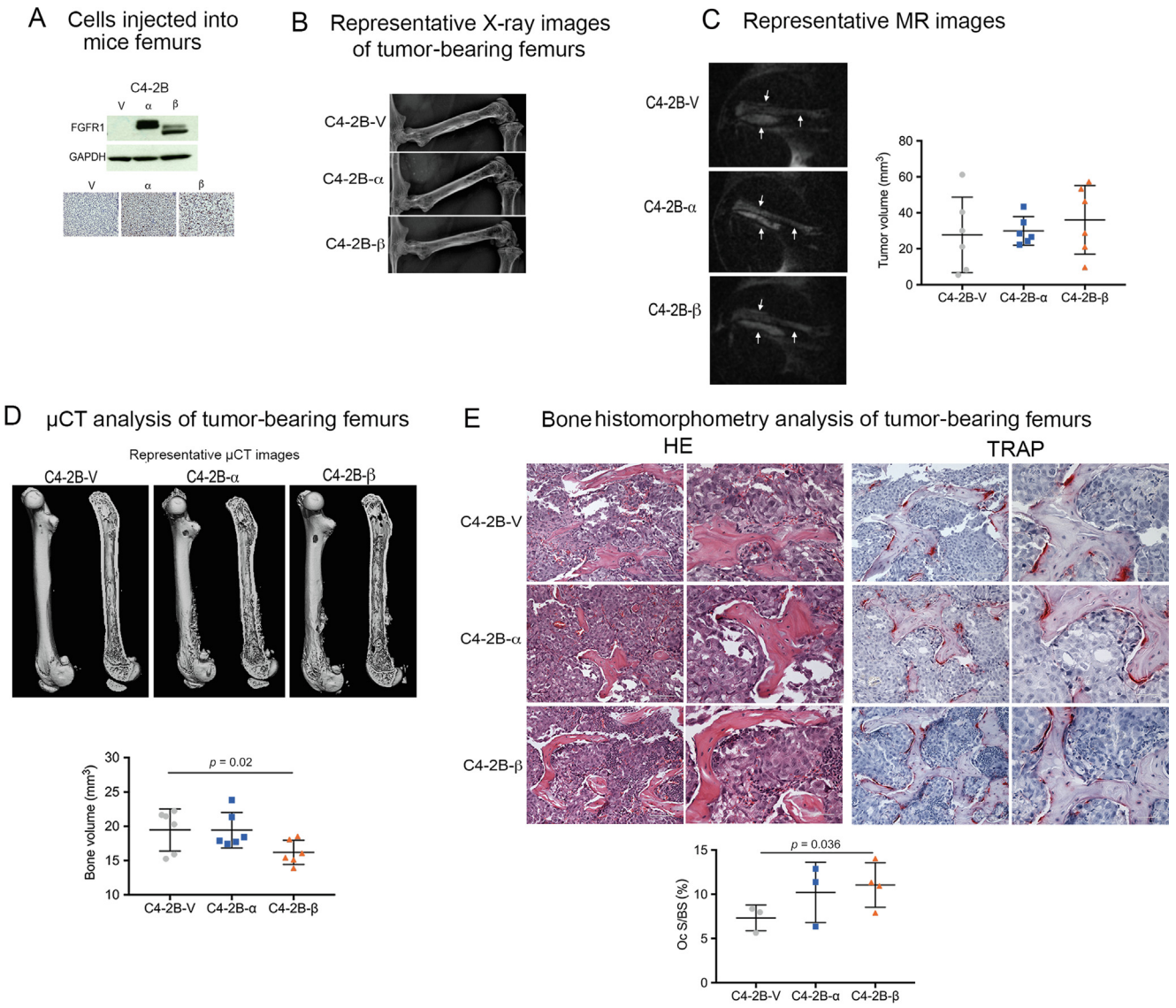

Fig. 3 – FGFR1 alters the bone phenotype induced by C4-2B cells in tumor-bearing femurs. (A) Western blot analysis and immunocytochemistry analysis results of FGFR1 expression in C4-2B cells injected into the femurs of mice (n = 6 per group). GAPDH was used as a loading control in the Western blot analysis. (B) Representative radiographs of x-ray analysis of femurs injected with C4-2B sublines at 8 wk after injection (given the slow growth rate of these cells *in vivo*). Owing to the mixed osteoblastic/osteolytic bone reaction produced by these cells, x-ray analysis could not be quantified accurately. (C) Representative sagittal MR images of femurs acquired as in Fig. 2C (left panels). Arrows indicate tumor. Tumor volume was assessed by MRI of C4-2B–FGFR1α, C4-2B–FGFR1β, or V tumor-bearing femurs (right panel). Student's t test; error bars indicate SD. (D) Representative two-dimensional slices of specimens analyzed by high-resolution µCT analysis at the end of study (upper panel). Bone volume results assessed by µCT analysis (lower panel). One-tailed Student's t test; error bars indicate SD. (E) Representative photomicrographs of decalcified tumor-bearing femur sections stained with HE (left panels) and tartrate-resistant acid phosphatase (TRAP; right panels; (20× magnification, left; 40× magnification, right). Bone histomorphometry analyses of TRAP-stained sections indicate an increase in osteoclast (OC) surface/bone surface in C4-2B–FGFR1β tumor-bearing mice (lower panel). Scale bar, 100 µm (20×) or 50 µm (40×). One-tailed Student's t test; error bars indicate SD. FGFR = fibroblast growth factor receptor; HE = hematoxylin and eosin; µCT = micro–computed tomography; MRI = magnetic resonance imaging; OC S/BS = osteoclast surface/bone surface; SD = standard deviation; V = empty vector.

LAD1 or controls (Supplementary Fig. 4A and 4B). As expected, the number of mice with bone metastases was higher among those injected with PC3-FGFR1β than among controls (Supplementary Fig. 4C, left). Further, a higher number of bone metastases per mouse was detected in the same group (p = 0.03; Supplementary Fig. 4C, right), which decreased with LAD1 silencing (PC3-FGFR1β shLAD1 vs PC3-FGFR1β Scr, p = 0.048; Supplementary Fig. 4D).

Furthermore, survival curves were associated negatively with LAD1 levels in the injected cells (p = 0.03; Supplementary Fig. 4E, left). We confirmed the contribution of LAD1 expression in mice survival by comparing this parameter in PC3-FGFR1β Scr (highest LAD1 levels by Western blot [WB]: 6.51)-injected mice with the combined survival data from the other three groups (PC3-V shLAD1, PC3-FGFR1β shLAD1, PC3-V Scr; LAD1 levels by WB: 0.06-1; p = 0.041; Supplementary Fig. 4E, right).

All these results support that FGFR1 reduces mice survival and increases bone metastasis, and suggest that LAD1 is one of the players in the FGFR1-induced PCa metastatic process.

Please cite this article as: E. Labanca, J. Yang, Peter D.A. Shepherd et al., Fibroblast Growth Factor Receptor 1 Drives the Metastatic Progression of Prostate Cancer, Eur Urol Oncol (2021), https://doi.org/10.1016/j.euo.2021.10.001

A

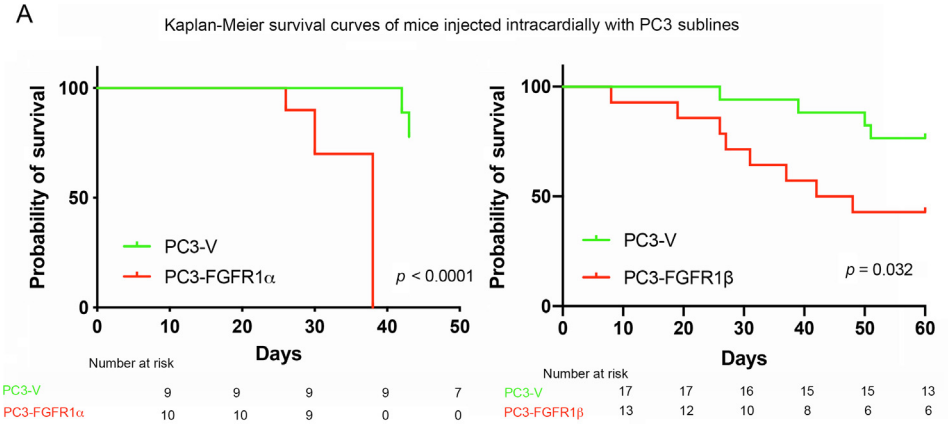

B

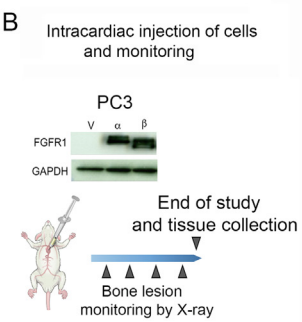

C Representative X-ray images of mice injected intracardially with PC3 sublines

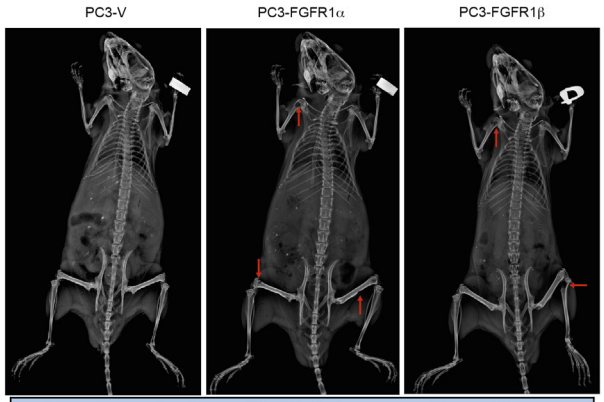

Number of mice with histology-confirmed bone metastases		
PC3-V	PC3-FGFR1α	PC3-FGFR1β
1/12 (8.3%)	11/12 (92%)	6/12 (50%)

D Representative radiolucent areas at the X-ray with corresponding microscopic analysis demonstrating tumor

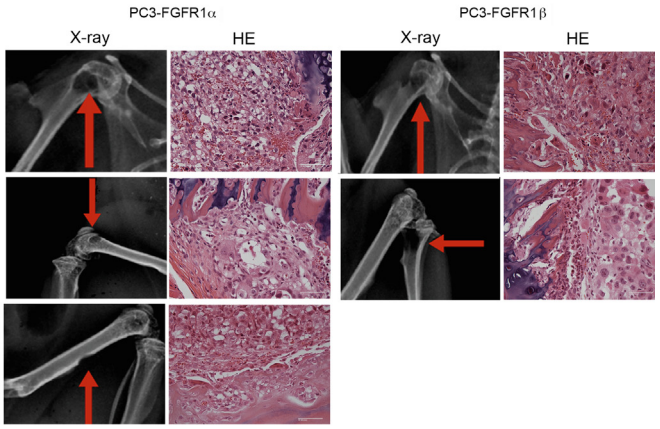

E Cells injected intracardially and monitoring

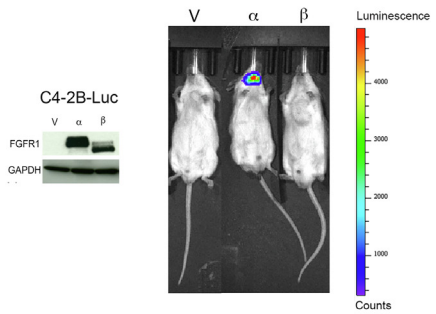

Number of mice with histology-confirmed bone metastases		
C4-2B-V	C4-2B-FGFR1α	C4-2B-FGFR1β
0/12 (0%)	2/12 (16%)	0/12 (0%)

F Representative MR images of bioluminescence area in E. with corresponding microscopic analysis demonstrating tumor

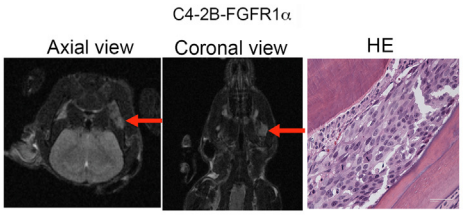

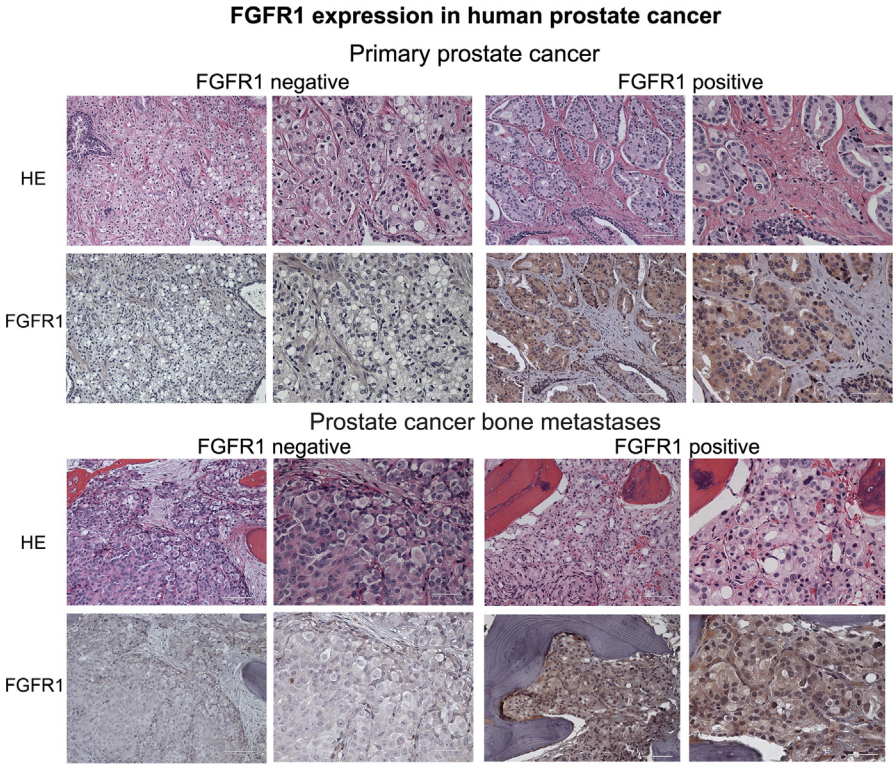

Summary of FGFR1 expression					
Primary prostate cancer (n = 29)			Prostate cancer bone metastases (n = 26)		
Negative	Positive/negative	Positive	Negative	Positive/negative	Positive
22/29 (76%)	5/29 (17%)	2/29 (6.9%)	8/26 (31%)	7/26 (27%)	11/26 (42%)

Fig. 5 – Significant increase in cases expressing FGFR1 in human prostate cancer bone metastases compared with primary disease. Representative photomicrograph images of sections stained with HE and immunostained with FGFR1 (20× and 40× magnification; scale bar 100 μm and 50 μm, respectively). The table summarizes FGFR1 expression findings in human primary prostate cancer and bone metastatic tissue samples assessed by immunohistochemical analysis (lower panel). Positive/negative (+/–) expression refers to weak positive staining (p = 0.0007, Fisher's exact test). FGFR = fibroblast growth factor receptor; HE = hematoxylin and eosin.

4. Discussion

Our comprehensive study of the biological role of two FGFR1 isoforms (α/β) and their associated signaling pathways in PCa underlies the importance of defining FGFR1 mediators of PCa progression and markers of FGFR1 signaling. This knowledge will help develop/optimize effective strategies for targeting FGFR1 as PCa therapy.

In addition to reporting that FGFR1 isoforms are associated with different genes and pathways in PCa, we show,

Fig. 4 – FGFR1 isoforms significantly increase prostate cancer bone metastases *in vivo*. (A) Kaplan-Meier survival curves and risk table of mice injected intracardially with PC3-FGFR1α (red, n = 10), FGFR1β (red, n = 14), and PC3 control cells (V, green; n = 9 and n = 17, right and left panel, respectively) in male CB17.SCID mice. Log-rank test. (B) Schematic representation of mice injected intracardially with PC3-FGFR1α, PC3-FGFR1β, or control empty vector (V) cells and monitoring by x-ray analysis (n = 12 per group). Western blot analysis results of FGFR1 expression in cells used in these studies. GAPDH was used as a loading control. (C) Representative radiographs of injected whole mice, illustrating radiolucent areas suspicious of osteolytic bone metastases (red arrows) at 4 wk after injection (upper panel). Number of mice with bone metastases after 4 wk of intracardiac injection (lower panel; p = 0.00005 FGFR1α vs V; p = 0.02 FGFR1β vs V, chi-square test). (D) Representative radiographs of radiolucent areas indicated by arrows in (C). Corresponding photomicrographs of decalcified tumor-bearing sections stained with HE (40× magnification, scale bar 50 μm) (E) Western blot analysis results of FGFR1 expression in C4-2B–FGFR1α, C4-2B–FGFR1β,or control empty vector (V) luciferase-expressing cells used for intracardiac injection (12 mice per group; upper left panel). GAPDH was used as a loading control. Metastatic lesions were monitored by bioluminescence imaging, with their precise locations identified by MRI and confirmed by histology at necropsy as depicted in (F). Representative images of signal detection monitored by ventral whole-body bioluminescence of mice at 12 wk after injection (upper right panel). Number of mice with bone metastases after 12 wk of intracardiac injection (lower panel). Mandibular metastases presented in two mice injected with C4-2B–FGFR1α. (F) MRI images of bioluminescent-positive area in the mouse shown in (E), acquired as in Fig. 2C (left and middle panels). Arrows indicate tumor at mandible. Corresponding photomicrographs of decalcified tumor-bearing sections stained with HE (40× magnification, scale bar 50 μm; right panel). FGFR = fibroblast growth factor receptor; HE = hematoxylin and eosin; MRI = magnetic resonance imaging; SD = standard deviation; V = empty vector.

Please cite this article as: E. Labanca, J. Yang, Peter D.A. Shepherd et al., Fibroblast Growth Factor Receptor 1 Drives the Metastatic Progression of Prostate Cancer, Eur Urol Oncol (2021), https://doi.org/10.1016/j.euo.2021.10.001

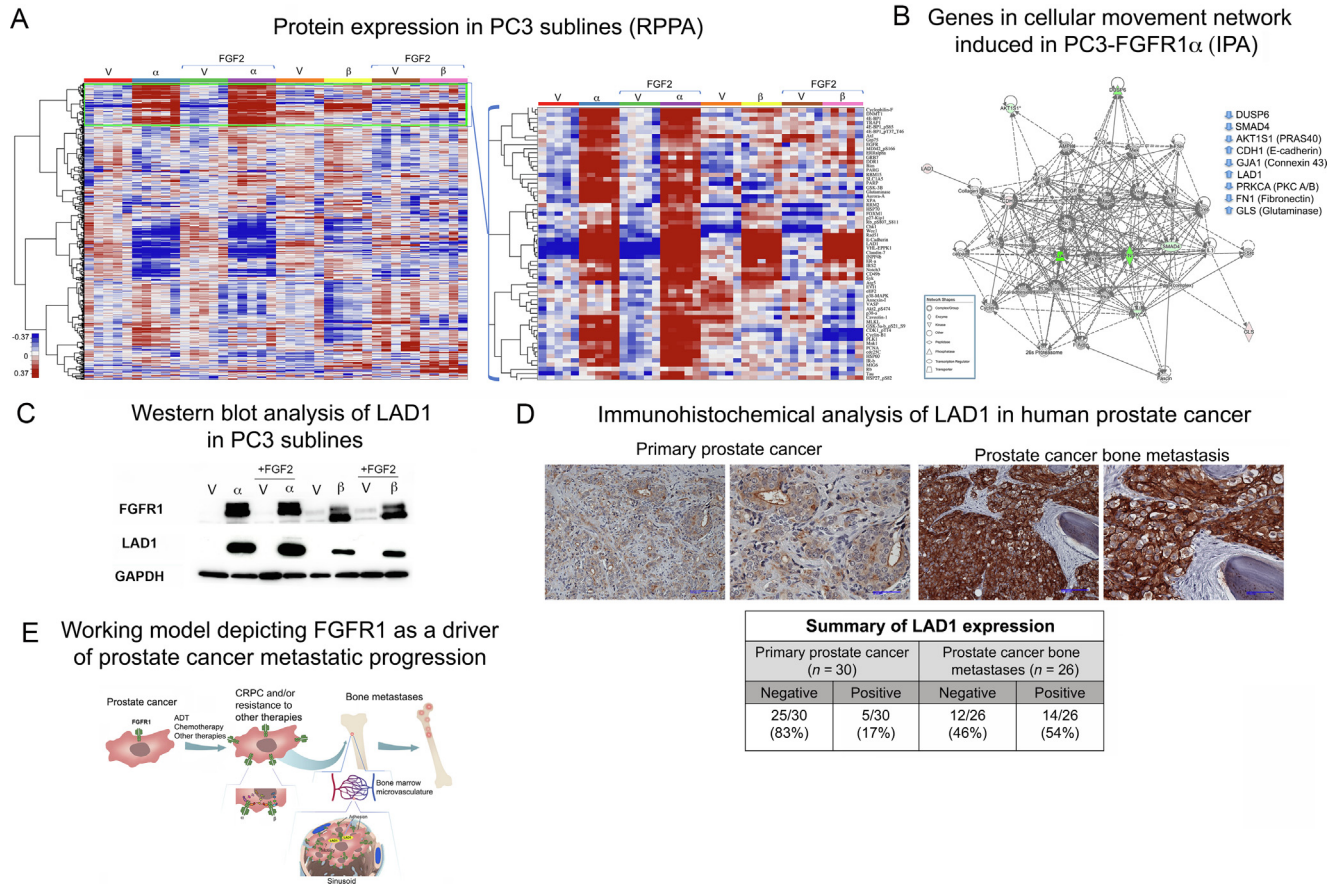

Summary of LAD1 expression			
Primary prostate cancer (n = 30)		Prostate cancer bone metastases (n = 26)	
Negative	Positive	Negative	Positive
25/30 (83%)	5/30 (17%)	12/26 (46%)	14/26 (54%)

Fig. 6 – FGFR1 induces ladinin 1 expression in PC3 prostate cancer cells. (A) Heatmap depicting antibody unsupervised hierarchical clustering of RPPA study results of PC3-FGFR1α, PC3-FGFR1β, and control (V) cells treated or untreated with FGF2 (left panel). Cell lysates were prepared as outlined in Fig. 1F. Each column represents a replicate (n = 5 per group). "Blue" color indicates that the values are above the median and "red" indicates that the values are below the median. Detailed view of section is outlined in green rectangle on left panel. (B) Network identified by Ingenuity Pathway Analysis (IPA) using RPPA analysis results of PC3-FGFR1α –induced genes. Similar findings were obtained with PC3-FGFR1β. (C) Expression levels of LAD1 in PC3 cells expressing FGFR1α, FGFR1β, or control empty vector (V), induced with FGF2. GAPDH was used as a loading control. (D) Representative photomicrograph images of sections immunostained with LAD1 (20× and 40× magnification). Table at the bottom summarizes LAD1 expression findings in untreated, nonmetastatic and in castration-resistant bone metastases (p = 0.005, Fisher's exact test). (E) A working model depicting FGFR1 as a driver of prostate cancer metastatic progression. Prostate cancer cells in advanced stages of the disease can exhibit significant lineage plasticity to evade therapeutic stress. Increased FGFR1 expression in prostate cancer cells may occur under selective pressure of chronic or short-term androgen deprivation therapy (ADT), second-generation androgen blockade, and/or other therapies (eg, cabozantinib) [7,38]. Alterations in FGFR-downstream pathways, such as PI3K/Akt and Src, have been implicated in the castration-resistant progression of prostate cancer [35,36]. Prostate cancer cells express various FGFR1 isoforms, for example, α and β, which activate common as well as different pathways. FGFR1 expression in therapy-resistant prostate cancer mediates growth of prostate cancer cells in bone and additional metastatic dissemination. Briefly, once prostate cancer cells overexpressing FGFR1 reach the bone marrow microvasculature, FGFR1-activated pathways, such as LAD1, would mediate motility and adhesion, enabling the prostate cancer to invade and grow in bone. As PCa progresses under current and upcoming targeted therapies, it is expected that the number of cases using FGFR as a pathway of progression will increase. Therefore, development of FGFR blockade for advanced PCa is imperative. CRPC = castration-resistant prostate cancer; FGF = fibroblast growth factor; FGFR = fibroblast growth factor receptor; LAD1 = ladinin 1; PCa = prostate cancer; RPPA = reverse-phase protein array.

for the first time, that FGFR1 expression in PCa cells enhances their metastatic behavior. These findings are in alignment with our discovery that FGFR1 expression is increased in CRPC bone metastases compared with primary, untreated disease.

Alterations in FGFR-downstream pathways (PI3K/Akt and Src) have been implicated in CRPC progression [35,36]. Furthermore, FGFR1 overcomes AR-dependent inhibition of cell proliferation in epithelial cells derived from differentiated Dunning R3327 adenocarcinomas [37].

Primary hormone-naïve/CRPC matched pairs showed FGFR1 transcript upregulation in CRPC [38]. This was confirmed (1) *in vitro*, where high FGFR1 expression was detected in bicalutamide-resistant LNCaP established by long- and short-term treatment; and (2) in clinical samples, by IHC analyses in hormone-naïve/CRPC matched samples, and associated with shorter time to relapse and reduced survival in CRPC [38].

A more recent report demonstrated that FGF signaling is capable of bypassing PCa AR dependence, in particular, in a subpopulation of patients following ADT and/or second-generation androgen blockade, characterized as "double-negative" due to the absence of both AR and neuroendocrine markers [8]. Notably, upregulation of the FGFR pathway occurred after AR ablation in PCa cells and PDX.

Our and others' findings [7,8,38] support the concept that, under selective pressure, FGFR1 pathway activation occurs later in the progression of the disease, mediating

therapy resistance. Therefore, the time frame of initiation of FGFR1 blockade therapy is of upmost relevance as a secondary prevention strategy.

Another important contribution of our studies was the identification of LAD1 as a downstream target of FGFR1. LAD1, a relatively uncharacterized protein, was implicated in mammary cancer cell motility [30]. Increased LAD1 predicted poor prognosis in patients with high-grade breast tumors [30], and was suggested as a new therapeutic target for triple-negative breast and ovarian cancers [31,32].

5. Conclusions

Our studies highlight the complexity of the FGFR pathway, and report for the first time the prometastatic effect of FGFR1 in AR-negative PCa cells and the enrichment of FGFR1 expression in CRPC bone metastases. Importantly, we identified LAD1 as a putative mediator of PCa metastases and/or marker of signaling activation (Fig. 6E). These findings are essential for the effective development of FGFR blockade as a therapy for advanced PCa.

The prometastatic effects of fibroblast growth factor receptor 1 (FGFR1) in prostate cancer emphasize the need to develop FGFR blockade as therapy for prostate cancer. FGFR1 isoforms and associated pathways reported in this study are essential to define the mediators of pathway activation and therapy resistance.

***Author contributions*:** Nora M. Navone had full access to all the data in the study and takes responsibility for the integrity of the data and the accuracy of the data analysis.

Study concept and design: Labanca, Yang, Navone.
Acquisition of data: Labanca, Yang, Wan, Shepherd, Dong, Bizzotto, Anselmino, Chinnaiyan, Broom.
Analysis and interpretation of data: Labanca, Starbuck, Guerra, Bizzotto, Anselmino, Ravoori, Kundra, Gueron, Troncoso, Navone.
Drafting of the manuscript: Labanca, Gueron, Navone.
Critical revision of the manuscript for important intellectual content: Corn, Logothethis.
Statistical analysis: Labanca, Broom, Navone.
Obtaining funding: Navone.
Administrative, technical, or material support: Navone.
Supervision: Navone.
Other: None.

Financial disclosures: Nora M. Navone certifies that all conflicts of interest, including specific financial interests and relationships and affiliations relevant to the subject matter or materials discussed in the manuscript (eg, employment/affiliation, grants or funding, consultancies, honoraria, stock ownership or options, expert testimony, royalties, or patents filed, received, or pending), are the following: None.

***Funding/Support and role of the sponsor*:** This work was supported in part by the Prostate Cancer Foundation, generous philanthropic contributions to The University of Texas MD Anderson Moon Shot Program, National Center Institute (NCI) Cancer Center Support Grant (P30CA16672), Cancer Center Prostate Cancer SPORE (National Institutes of Health [NIH]/NCI P50 CA140388-08), DOD-PCRP (W81XWH-14-1-0554), Janssen Pharmaceutical Companies of Johnson & Johnson, and the David H. Koch Center for Applied Research in Genitourinary Cancers at MD Anderson, Houston, TX. Bradley M. Broom was supported in part by NIH/NCI grants 5U24CA199461, 5P30CA016672, and 2P50CA140388-06A1.

***Data sharing*:** Materials are available through a material transfer agreement, and data are freely available.

***Acknowledgments*:** We thank Charles V. Kingsley for technical assistance in the i.c. injection, the Small Animal Imaging Facility personnel at MDACC for technical support, Brian C. Dawson for CT analysis, Sarah E. Townsend for editing the manuscript, Elba S. Vazquez for helpful advice and criticism, Jordan T. Pietz for scientific illustrations, and the Rolanette and Berdon Lawrence Bone Disease Program of Texas.

Appendix A. Supplementary data

Supplementary data to this article can be found online at https://doi.org/10.1016/j.euo.2021.10.001.

References

[1] Watson PAA, Arora VK, Sawyers CL. Emerging mechanisms of resistance to androgen receptor inhibitors in prostate cancer. Nat Rev Cancer 2015;15:701–11.
[2] Corn PG, Wang F, McKeehan WL, Navone N. Targeting fibroblast growth factor pathways in prostate cancer. Clin Cancer Res 2013;19:5856–66.
[3] Li ZG, Mathew P, Yang J, et al. Androgen receptor-negative human prostate cancer cells induce osteogenesis in mice through FGF9-mediated mechanisms. J Clin Invest 2008;118:2697–710.
[4] Valta MP, Tuomela J, Bjartell A, Valve E, Vaananen HK, Harkonen P. FGF-8 is involved in bone metastasis of prostate cancer. Int J Cancer 2008;123:22–31.
[5] Labanca E, Vazquez ES, Corn PG, et al. Fibroblast growth factors signaling in bone metastasis. Endocr Relat Cancer 2020;27:R255–65.
[6] Wan X, Corn PG, Yang J, et al. Prostate cancer cell-stromal cell crosstalk via FGFR1 mediates antitumor activity of dovitinib in bone metastases. Sci Transl Med 2014;6, 252ra122.
[7] Varkaris A, Corn PG, Parikh NU, et al. Integrating murine and clinical trials with cabozantinib to understand roles of MET and VEGFR2 as targets for growth inhibition of prostate cancer. Clin Cancer Res 2016;22:107–21.
[8] Bluemn EG, Coleman IM, Lucas JM, et al. Androgen receptor pathway-independent prostate cancer is sustained through FGF signaling. Cancer Cell 2017;32, 474–89.e6.
[9] Vickers SM, Huang ZQ, MacMillan-Crow L, Greendorfer JS, Thompson JA. Ligand activation of alternatively spliced fibroblast growth factor receptor-1 modulates pancreatic adenocarcinoma cell malignancy. J Gastrointest Surg 2002;6:546–53.
[10] Bruno IG, Jin W, Cote GJ. Correction of aberrant FGFR1 alternative RNA splicing through targeting of intronic regulatory elements. Hum Mol Genet 2004;13:2409–20.
[11] Tomlinson DC, Knowles MA. Altered splicing of FGFR1 is associated with high tumor grade and stage and leads to increased sensitivity to FGF1 in bladder cancer. Am J Pathol 2010;177:2379–86.
[12] Zhao M, Zhuo ML, Zheng X, Su X, Meric-Bernstam F. FGFR1beta is a driver isoform of FGFR1 alternative splicing in breast cancer cells. Oncotarget 2019;10:30–44.
[13] Wendt MK, Taylor MA, Schiemann BJ, Sossey-Alaoui K, Schiemann WP. Fibroblast growth factor receptor splice variants are stable markers of oncogenic transforming growth factor beta1 signaling in metastatic breast cancers. Breast Cancer Res 2014;16:R24.
[14] Morrison RS, Yamaguchi F, Saya H, et al. Basic fibroblast growth factor and fibroblast growth factor receptor I are implicated in the growth of human astrocytomas. J Neurooncol 1994;18:207–16.
[15] Yamaguchi F, Saya H, Bruner JM, Morrison RS. Differential expression of two fibroblast growth factor-receptor genes is

associated with malignant progression in human astrocytomas. Proc Natl Acad Sci U S A 1994;91:484–8.
[16] Karajannis MA, Vincent L, Direnzo R, et al. Activation of FGFR1beta signaling pathway promotes survival, migration and resistance to chemotherapy in acute myeloid leukemia cells. Leukemia 2006;20:979–86.
[17] Alizadeh M, Gelfman CM, Bench SR, Hjelmeland LM. Expression and splicing of FGF receptor mRNAs during APRE-19 cell differentiation in vitro. Invest Ophthalmol Vis Sci 2000;41:2357–62.
[18] Prudovsky IA, Savion N, LaVallee TM, Maciag T. The nuclear trafficking of extracellular fibroblast growth factor (FGF)-1 correlates with the perinuclear association of the FGF receptor-1alpha isoforms but not the FGF receptor-1beta isoforms. J Biol Chem 1996;271:14198–205.
[19] Palanisamy N, Yang J, Shepherd PDA, et al. The MD Anderson prostate cancer patient-derived xenograft series (MDA PCa PDX) captures the molecular landscape of prostate cancer and facilitates marker-driven therapy development. Clin Cancer Res 2020;26:4933–46.
[20] Pin E, Federici G, Petricoin 3rd EF. Preparation and use of reverse protein microarrays. Curr Protoc Protein Sci 2014;75:27.7.1–9.
[21] Abeshouse A, Ahn J, Akbani R, et al. The molecular taxonomy of primary prostate cancer. Cell 2015;163:1011–25.
[22] Abida W, Cyrta J, Heller G, et al. Genomic correlates of clinical outcome in advanced prostate cancer. Proc Natl Acad Sci U S A 2019;116:11428–36.
[23] Broom BM, Ryan MC, Brown RE, et al. A galaxy implementation of next-generation clustered heatmaps for interactive exploration of molecular profiling data. Cancer Res 2017;77:e23.
[24] Ryan MC, Cleland J, Kim R, Wong WC, Weinstein JN. SpliceSeq: a resource for analysis and visualization of RNA-Seq data on alternative splicing and its functional impacts. Bioinformatics 2012;28:2385–7.
[25] Subramanian A, Tamayo P, Mootha VK, et al. Gene set enrichment analysis: a knowledge-based approach for interpreting genome-wide expression profiles. Proc Natl Acad Sci U S A 2005;102:15545–50.
[26] Kassambara A, Kosinski M, Biecek P. survminer: Drawing survival curves using "ggplot2". https://rpkgs.datanovia.com/survminer/.
[27] Johnson DE, Williams LT. Structural and functional diversity in the FGF receptor multigene family. Adv Cancer Res 1993;60:1–41.
[28] McKeehan WL, Wang F, Kan M. In: Progress in nucleic acid research and molecular biology. Press: Academic; 1997. p. 135–76.
[29] Navone NM, van Weerden WM, Vessella RL, et al. Movember GAP1 PDX project: an international collection of serially transplantable prostate cancer patient-derived xenograft (PDX) models. Prostate 2018;78:1262–82.
[30] Roth L, Srivastava S, Lindzen M, et al. SILAC identifies LAD1 as a filamin-binding regulator of actin dynamics in response to EGF and a marker of aggressive breast tumors. Sci Signal 2018;11:eaan0949.
[31] Wang X, Guda C. Integrative exploration of genomic profiles for triple negative breast cancer identifies potential drug targets. Medicine (Baltimore) 2016;95:e4321.
[32] Santin AD, Zhan F, Bellone S, et al. Gene expression profiles in primary ovarian serous papillary tumors and normal ovarian epithelium: identification of candidate molecular markers for ovarian cancer diagnosis and therapy. Int J Cancer 2004;112:14–25.
[33] Putzke AP, Ventura AP, Bailey AM, et al. Metastatic progression of prostate cancer and e-cadherin regulation by zeb1 and SRC family kinases. Am J Pathol 2011;179:400–10.
[34] Twum-Ampofo J, Fu DX, Passaniti A, Hussain A, Siddiqui MM. Metabolic targets for potential prostate cancer therapeutics. Curr Opin Oncol 2016;28:241–7.
[35] Acevedo VD, Ittmann M, Spencer DM. Paths of FGFR-driven tumorigenesis. Cell Cycle 2009;8:580–8.
[36] Zhu M-L, Kyprianou N. Androgen receptor and growth factor signaling cross-talk in prostate cancer cells. Endocrine Relat Cancer 2008;15:841–9.
[37] Kobayashi M, Huang Y, Jin C, et al. FGFR1 abrogates inhibitory effect of androgen receptor concurrent with induction of androgen-receptor variants in androgen receptor-negative prostate tumor epithelial cells. Prostate 2011;71:1691–700.
[38] Armstrong K, Ahmad I, Kalna G, et al. Upregulated FGFR1 expression is associated with the transition of hormone-naive to castrate-resistant prostate cancer. Br J Cancer 2011;105:1362–9.

Please cite this article as: E. Labanca, J. Yang, Peter D.A. Shepherd et al., Fibroblast Growth Factor Receptor 1 Drives the Metastatic Progression of Prostate Cancer, Eur Urol Oncol (2021), https://doi.org/10.1016/j.euo.2021.10.001